



1

2

3 Climatic factors contributing to long-term variations of fine dust concentration in the
4 United States

5

6 Bing Pu^{1,2} and Paul Ginoux²

7 ¹Atmospheric and Oceanic Sciences Program, Princeton University,

8 Princeton, New Jersey 08544

9 ²NOAA Geophysical Fluid Dynamics Laboratory, Princeton, New Jersey 08540

10

11

12

13

14

15

16

17

18

19

20

21

22 *Correspondence to:* Bing Pu (bpu@princeton.edu)

23



24 **Abstract.** High concentration of dust particles can cause respiratory problems and
25 increase non-accidental mortality. Studies found fine dust (with aerodynamic diameter
26 less than 2.5 microns) is an important component of the total PM_{2.5} mass in the western
27 and central U.S. in spring and summer and has positive trends. This work examines
28 factors influencing long-term variations of fine dust concentration in the U.S. using
29 station data from the Interagency Monitoring Protected Visual Environments
30 (IMPROVE) network during 1990-2015. The variations of the fine dust concentration can
31 be largely explained by the variations of precipitation, surface bareness, and 10 m wind
32 speed. Moreover, including convective parameters such as convective inhibition (CIN)
33 and convective available potential energy (CAPE) better explains the variations and
34 trends over the Great Plains from spring to fall.

35 While the positive trend of fine dust concentration in the Southwest in spring is
36 associated with precipitation deficit, the increasing of fine dust over the central Great
37 Plains in summer is largely associated with an enhancing of CIN and a weakening of
38 CAPE, which are related to increased atmospheric stability due to surface drying and
39 lower troposphere warming. The positive trend of the Great Plains low-level jet also
40 contributes to the increasing of fine dust concentration in the central Great Plains in
41 summer via its connections with surface winds and CIN.

42 Summer dusty days in the central Great Plains are usually associated with a
43 westward extension of the North Atlantic subtropical high that intensifies the Great Plains
44 low-level jet and also results in a stable atmosphere with subsidence and reduced
45 precipitation.

46



47 **1. Introduction**

48 Mineral dust is one of the most abundant atmospheric aerosols by mass. It is lifted
49 to the atmosphere by strong wind from dry and bare surfaces. Severe dust storms have
50 far-reaching socioeconomic impacts, affecting public transportation and health (e.g.,
51 Morman and Plumlee, 2013) by degrading visibility, causing traffic accidents, breathing
52 problems, and lung diseases. Dust storms are found to be associated with increases in
53 non-accidental mortality in the U.S. during 1993-2005 (Crooks et al., 2016).

54 Major dust sources in the United States are located over the western U.S., where
55 several deserts are located, e.g., the Mojave, Sonoran, and northern Chihuahuan deserts,
56 and over the central U.S., where the dust sources are largely anthropogenic, in association
57 with agriculture activities (Ginoux et al., 2012). Climate models project a drying trend in
58 the late half of the twenty-first century over the southwest and central U.S. (e.g., Seager
59 et al., 2007; Cook et al., 2015), regions largely collocated with the major dust sources in
60 the U.S. This raises questions such as how future dust activities will change in the U.S.
61 To project future dust variations, we first need to understand how dust activity varies in
62 the present day. Pu and Ginoux (2017) explored this question using dust optical depth
63 (DOD) derived from MODIS Deep Blue (M-DB2) aerosol products during 2003-2015
64 and found that variations of dust activity are largely associated with precipitation, near
65 surface wind speed, and surface bareness.

66 While DOD describes the total optical depth of dust aerosols with different sizes
67 and is widely used to study climate-dust interactions, fine dust with aerodynamic
68 diameter less than 2.5 μm is more frequently used for air quality purposes. The diameter
69 of dust aerosols usually ranges from 0.1 to 50 μm (Duce, 1995), with measured volume



70 median diameters varying from 2.5 to 9 μm (Reid et al., 2003) and clay (diameter < 2 μm
71) mass fraction representing less than 10% (Kok, 2011). In terms of air quality, fine dust
72 contributed about 40-50% of total Particulate Matter 2.5 (PM_{2.5}) mass over the
73 southwestern U.S. in spring and about 20-30% over the southwestern to central U.S. in
74 summer (Hand et al., 2017).

75 Stations in the network of the Interagency Monitoring of Protected Visual
76 Environments (IMPROVE) have collected PM_{2.5} samples in the U.S. since 1988 (Malm
77 et al., 1994; Hand et al., 2011). Analysis of chemical elements is used to derive fine dust
78 concentration. Due to its long temporal coverage, this dataset has been widely used to
79 study long-term variations of fine dust in the U.S. Using IMPROVE data, Hand et al.
80 (2016) found an increasing trend of fine dust in spring in the southwestern U.S. during
81 1995-2014 and related this trend to a negative Pacific decadal oscillation (PDO) from
82 2007 to 2014. Tong et al. (2017) also found a rapid increase of dust storm activity in the
83 Southwest from 1988 to 2011 and related the trend to sea surface temperature variations
84 in the Pacific. Later, Hand et al. (2017) examined the trends of IMPROVE fine dust
85 concentration in different seasons from 2000 to 2014 and found positive trends over the
86 southwestern U.S. in spring and over the central U.S. in summer and fall. Similarly,
87 Zhang et al. (2017) also found a positive trend of fine dust over the central U.S. from
88 2005 to 2015 and suggested this trend may contribute to the increase of absorbing aerosol
89 optical depth in the region. Nonetheless, the possible causes of the fine dust trends,
90 especially the increase of fine dust over the central U.S., have not been thoroughly
91 discussed by previous studies. Here, we explore the underlying factors driving the long-
92 term variations of fine dust from 1990 to 2015. We start with local environmental factors



93 and then examine the possible influence of the low-level jet over the Great Plains on fine
94 dust concentration in summer.

95 The following section describes the data and analysis method used in the paper.
96 Section 3 presents our major results and conclusions are summarized in Section 4.

97

98 **2. Data and Methodology**

99 **2.1 IMPROVE fine dust**

100 IMPROVE stations are located in National Parks and wilderness areas in the
101 United States, with PM_{2.5} sampling performed every third day since March 1988.
102 Records from 204 stations within a domain of 15°-53°N and 60°-127°W are used in this
103 study, and most of the stations contain data longer than 10 years (Fig. S1 in the
104 Supplement). Elemental concentration is determined from X-ray fluorescence, and fine
105 dust concentration is calculated using the concentrations of aluminum (Al), silicon (Si),
106 calcium (Ca), iron (Fe), and titanium (Ti) by assuming oxide norms associated with
107 predominant soil species (Malm et al., 1994; their Eq. 5). More details regarding
108 IMPROVE stations, sampling, and analysis method can be found in previous studies
109 (Hand et al., 2011;2012; 2016;2017).

110 We averaged daily station data to monthly means and then interpolated them to a
111 0.5° by 0.5° grid using inverse distance weighted interpolation, i.e., weights depending
112 on the inverse cubic distance between the site location and the interpolated grid point. In
113 daily composite analysis, daily station data are interpolated to a 0.5° by 0.5° grid using
114 the same method.



115 Following Pu and Ginoux (2017), several dusty regions are selected for analysis.
116 The southwestern U.S. (WST for short; 32°-42°N, 105°-124°W) and Great Plains (GP for
117 short; 25°-49°N, 95°-105°W) cover the major dust source regions (black boxes in Fig. 1),
118 while the central Great Plains (32°-40°N, 95°-102°W) is chosen to examine the
119 increasing trend of fine dust in the region.

120

121 **2.2 Cloud-Aerosol Lidar with Orthogonal Polarization (CALIOP) products**

122 CALIOP is the two-wavelength polarization lidar carried by Cloud-Aerosol Lidar
123 and Infrared Pathfinder Satellite Observation (CALIPSO) satellite, which was launched
124 in April 2006 (Winker et al., 2004;2007). CALIOP measures backscattered radiances
125 attenuated by the presence of aerosols and clouds, whose microphysical and optical
126 properties are retrieved. Daily products are available since June 2006. To examine the
127 vertical profile of dust concentration in the U.S., the daily 532 nm total attenuated
128 backscatter from Level 1 product and depolarization ratio from Level 2 product are used.
129 Depolarization ratio can be used to separate spherical and non-spherical hydrometeors
130 and aerosols (Sassen, 1991), and here ≥ 0.2 is used to separate non-spherical dust from
131 other aerosols (Li et al., 2010).

132

133 **2.2 Precipitation**

134 The Precipitation Reconstruction over Land (PRECL; Chen et al., 2002) from the
135 National Oceanic and Atmospheric Administration (NOAA) is a global analysis available
136 monthly from 1948 to present at a 1° by 1° resolution, and is suitable to study long-term
137 connections between fine dust and precipitation. The dataset is derived from gauge



138 observations from the Global Historical Climatology Network (GHCN), version 2, and
139 the Climate Anomaly Monitoring System (CAMS) datasets. Monthly precipitation from
140 1990 to 2015 is used.

141

142 **2.3 Leaf area index (LAI)**

143 Monthly LAI derived from the version 4 of Climate Data Record (CDR) of
144 Advanced Very High Resolution Radiometer (AVHRR) surface reflectance (Claverie et
145 al., 2014) and produced by the National Aeronautics and Space Administration (NASA)
146 Goddard Space Flight Center (GSFC) and the University of Maryland is used. The
147 gridded monthly data are on a 0.05° by 0.05° horizontal resolution and available from
148 1981 to present. This dataset is selected due to its high spatial resolution and long
149 temporal coverage. Monthly data from 1990 to 2015 are used. A detailed discussion on
150 the algorithm and evaluation of the dataset can be found by Claverie et al. (2016).

151 Surface bareness is derived from seasonal mean LAI, and is calculated following
152 Pu and Ginoux (2017),

$$153 \quad \text{Bareness} = -\exp(\text{LAI}) \quad . \quad (1)$$

154

155 **2.4 Reanalysis**

156 North American Regional Reanalysis (NARR; Mesinger et al., 2006) provides 3-
157 hourly, daily, and monthly meteorological variables from 1979 to the present at a high
158 spatial resolution (i.e., about 32km horizontally). Precipitation in the NARR is
159 assimilated with observations. The reanalysis reasonably captures the hydroclimatic
160 fields in the continental U.S. on multiple time scales (Ruiz-Barradas and Nigam, 2006;



161 Ruane, 2010a, b), thus is suitable to study the connection between fine dust concentration
162 and local hydroclimatic variables. Here daily and monthly convective variables such as
163 convective inhibition (CIN), and convective available potential energy (CAPE) are used.
164 CIN is defined as the energy that a parcel needs to overcome to rise above the level of
165 free convection (LFC), and is usually written as:

$$166 \quad \text{CIN} = - \int_{P_{\text{sf}c}}^{P_{\text{LFC}}} R_d (T_{vp} - T_{ve}) d \ln p \quad , \quad (2)$$

167 where P_{LFC} is the pressure at LFC, $P_{\text{sf}c}$ is the pressure at the surface, R_d is the specific gas
168 constant for dry air, T_{vp} is the virtual temperature of the lifted parcel, and T_{ve} is the virtual
169 temperature of the environment. By definition, CIN is usually a negative variable, with
170 bigger CIN (in absolute value) indicating greater inhibition. On the other hand, CAPE
171 describes the positive buoyancy of an air particle from the LFC to the equilibrium level
172 (neutral buoyancy), and can be written as:

$$173 \quad \text{CAPE} = - \int_{P_{\text{LFC}}}^{P_{\text{EL}}} R_d (T_{vp} - T_{ve}) d \ln p \quad , \quad (3)$$

174 where P_{EL} is the pressure at the equilibrium level. Both CIN and CAPE describe the
175 stability of the atmosphere, and usually convection easily occurs when CAPE is high and
176 CIN is low (in absolute value; e.g., Colby, 1984; Riemann-Campe et al., 2009; Myoung
177 and Nielsen-Gammon, 2010a). Note the two variables can sometimes vary in opposite
178 directions. Indeed, when CAPE is high, strong inhibition may still prohibit the occurrence
179 of deep convection.

180 In addition, daily and monthly means of horizontal wind speed at 900 hPa,
181 temperature at 700 hPa (T_{700}), 10 m wind speed, dew point temperature (T_{dp}), and 2 m air
182 temperature (T_{2m}), total cloud cover, total and convective precipitation are used.



183 Another reanalysis used in this work is the ERA-Interim (Dee et al., 2011) from
184 the European Centre for Medium-Range Weather Forecasts (ECMWF). ERA-Interim is a
185 global reanalysis with a horizontal resolution of T255 (about 0.7° or 80 km) and 37
186 vertical levels, available from 1979 to present. It complements the regional reanalysis by
187 providing a larger domain to analyze circulation variations and also a few surface
188 variables that are not available in the NARR. 6-hourly analysis and 3-hourly forecast
189 variables such as surface turbulence stress, vertical and horizontal winds, air temperature,
190 and specific humidity from 1000 to 200 hPa, 850 hPa winds and geopotential height are
191 used to calculate daily means of these variables.

192

193 **2.5 Multiple-linear regression**

194 To understand the connection between the potentially controlling factors and the
195 variation of fine dust concentration, multiple-linear regressions are applied by regressing
196 the observed gridded fine dust concentration onto 3, 4, or 5 standardized controlling
197 factors, a method similar to the one used by Pu and Ginoux (2017). Here all data are
198 interpolated to a 1° by 1° grid for the regression analysis. The fine dust concentration is
199 then reconstructed by using the regression coefficients and observed variations of the
200 controlling factors (such as precipitation, surface wind, and bareness). We focus our
201 analysis on two statistical properties: correlations of regional averaged time series and
202 pattern correlations for the trends. These two properties are calculated for both observed
203 and regression model estimated (i.e., reconstructed) fine dust concentrations.

204

205 **3. Results**



206 **3.1 Trends of surface fine dust concentration during 1990-2015 and local controlling**
207 **factors**

208 Figure 1 shows the trend of fine dust concentration from gridded data (shading)
209 and also those from stations with at least 23 years of consecutive records (colored circles)
210 from 1990 to 2015. Significant positive trends are found over the southwestern U.S. in
211 spring (MAM), over the central to southern Great Plains in summer (JJA), and the
212 northern Great Plains in fall (SON). Dust concentration also increases over southwestern
213 Arizona (up to $0.06 \mu\text{g m}^{-3} \text{ yr}^{-1}$), by about 2.5% of its climatological value (Fig. S2 in the
214 Supplement) per year, in all seasons. A similar increasing trend of fine dust in southern
215 Arizona in spring from 1988 to 2009 is also noticed by Sorooshian et al. (2011). A
216 decreasing trend is found over the northeastern U.S. in all seasons as well. The pattern is
217 somewhat similar to the trend identified by Hand et al. (2017; their Fig. 9) for 2000-2014,
218 who also found increasing trends of fine dust in the Southwest in spring and the central
219 Great Plains in summer.

220 As suggested by previous studies, the trend of fine dust may be biased due to
221 suspicious trends in some chemical species (Al, Si, and Ti) used to construct fine dust in
222 association with changes of analytical methods (e.g., Hyslop et al., 2015; Hand et al.,
223 2016; Hand et al., 2017). Fe has been suggested as a good proxy of fine dust since it's
224 more stable and is a key component of dust (Hand et al. 2016; 2017). We examined the
225 trend of fine Fe (Fig. S3 in the Supplement), and found the pattern is very similar to the
226 trend of fine dust. In fact, we found the correlations between seasonal mean fine dust and
227 Fe (both gridded data and long-term stations) are around 0.90 (significant at the 99%
228 confidence level) in most part of the U.S. during 1990-2015 (Fig. S4 in the Supplement).



229 This suggests the trends revealed directly from fine dust record are comparably reliable
230 as those calculated from Fe. So we use fine dust concentration for this analysis.

231 What are the dominant factors influencing the variations of fine dust
232 concentration? Hand et al. (2016) found that the PDO played an important role in the
233 variability of fine dust concentration over the Southwest in March by creating a windier,
234 drier, and less vegetated environment. We would like to extend their analysis to other
235 seasons and regions. In addition, we focus on identifying key controlling factors at the
236 local level because remote forcings such as the PDO influence dust variations through
237 their tele-connection with local controlling factors. Pu and Ginoux (2017) found that
238 local precipitation, surface bareness, and surface wind speed could explain 49% to 88%
239 of the variances of dust event frequency (derived from DOD) over the western U.S. and
240 the Great Plains in different seasons from 2003 to 2015. We first examine to what extent
241 these factors can explain the variance of near surface fine dust concentration. Similar to
242 Pu and Ginoux (2017), we do not separate the contribution from local emissions or
243 remote transportation to the fine dust concentration, although contributions from Asian
244 dust in spring over the western U.S. (Fischer et al., 2009; Creamean et al., 2014; Yu et al.,
245 2012) and from North African dust in summer over the southeastern U.S. (Perry et al.,
246 1997; Prospero, 1999b) have been observed.

247 Figure 2a-d shows the dominant controlling factor among the three (precipitation,
248 surface wind, and bareness) for fine dust concentration variations at each grid point.
249 Precipitation plays an important role in most parts of the southern U.S. in winter. In
250 spring, surface wind starts to dominate the variations of fine dust along the Gulf coast and
251 eastern Great Plains, consistent with the intensification of the Great Plains low-level jet



252 (e.g., Helfand and Schubert, 1995; Weaver and Nigam, 2008; Pu and Dickinson, 2014; Pu
253 et al., 2016) in April and May, while bareness is important over the western Great Plains
254 and the Midwest. During summer, the influence of surface wind speed gets stronger,
255 especially over western Arizona and the lower Mississippi basin, whereas bareness and
256 precipitation are also important in many parts of the Great Plains and western U.S.
257 Precipitation becomes the dominant factor over most parts of the U.S. again in fall, with
258 surface winds playing a weak role over the southeast and northeast coasts.

259 The regression coefficients obtained here share some similarity with those shown
260 by Pu and Ginoux, (2017; their Fig 4) using DOD, e.g., the importance of surface
261 bareness in the Great Plains in spring and summer. However, there are also quite large
262 differences, likely due to different periods of regression and the fact that the DOD and
263 surface fine dust concentration are not always linearly related to each other (Fig. S5 in the
264 Supplement). For instance, over the Great Plains and the southwestern U.S., seasonal
265 mean fine dust is linearly related to the DOD in spring but not so in summer. As
266 mentioned earlier, fine dust covers a small fraction of the total mass distribution of dust
267 particles, thus the connections between fine dust concentration and the controlling factors
268 could be different from those with the DOD. For example, the scavenging effect of
269 precipitation is more efficient on small particles (e.g., Zender et al., 2003) and as a result
270 precipitation generally plays an overall more important role on fine dust variations than
271 on the DOD, especially in winter, spring, and fall.

272 The correlations between reconstructed fine dust concentration in the
273 southwestern U.S. (using regression coefficients and observed variations of precipitation,
274 surface wind, and bareness) and that from the IMPROVE range from 0.69 in fall to 0.82



275 in winter, indicating that the above three factors explain about 48% to 67% variances of
276 fine dust in the Southwest from 1990 to 2015. Over the Great Plains, correlations
277 between the reconstructed and observed fine dust concentration ranges from 0.57 in
278 summer to 0.69 in winter, explaining 32% to 48% variances statistically, lower than over
279 the Southwest.

280 The pattern correlations between the observed trend and the trend from
281 reconstructed fine dust are all above 0.80 in the Southwest except in the summer, whereas
282 in the Great Plains region, the pattern correlations are much lower, from 0.06 in fall to
283 0.48 in winter. In fact, the reconstructed trend missed the observed positive trend of fine
284 dust over the central Great Plains in summer (not shown). This is consistent with the low
285 confidence level of the regression coefficients over the central Great Plains in summer
286 (Fig. 2c) and indicates that the above three factors are not sufficient to well explain the
287 variations of fine dust in the central Great Plains.

288 The development of dust storms has long been related to convection and
289 atmospheric stability (e.g., Marsham et al., 2008; Cuesta et al., 2009). Here we examine
290 whether the variances of fine dust concentration and trend can be better represented by
291 adding CIN (i.e., four-factor) and both CIN and CAPE (i.e., five-factor) in addition to the
292 three factors (i.e., three-factor) discussed above.

293 Figure 2e shows correlations (blue bars) between the observed and the
294 reconstructed regional mean fine dust concentration from three-, four-, and five-factor
295 regressions, and corresponding pattern correlations (pink dots) between trends from the
296 observed and reconstructed fine dust for the Great Plains and the southwestern U.S. In
297 both regions, correlations of interannual variation between the reconstructed and



298 observed fine dust are slightly improved from three-factor regression to five-factor
299 regression. Pattern correlations are largely improved over the Great Plains when
300 including CIN and CAPE, especially in spring (from 0.30 to 0.89) and summer (from
301 0.34 to 0.93), although slightly decreased in winter, whereas the improvement of pattern
302 correlations in the Southwest is much weaker.

303 The collinearity among the factors used in the multiple linear regression can be
304 examined by the variance inflation factor (VIF; O'Brien, 2007; Abudu et al., 2011), and
305 usually values between 5 and 10 are considered high collinearity and the results of
306 regression are less reliable. Increasing the number of predictors in multiple linear
307 regression generally increase VIFs. The VIFs for three-factor regression are around 1 and
308 2 in most areas, with a few spots around 3 (not shown), while the VIFs for five-factor
309 regression are slightly higher, especially for CIN and CAPE over the Southwest (Figs. S6
310 and 7 in the Supplement). The increase of VIF and relatively weak improvement in the
311 correlations in the Southwest when adding the convective factors suggest that three
312 factors (precipitation, surface wind and bareness) are sufficient to capture the variations
313 and trend of fine dust in the region. Over the Great Plains, adding CIN and CAPE can
314 better explain the variations.

315 We now examine key factors driving the observed positive trends of fine dust
316 concentration in spring and summer, the dustiest seasons (Fig. S2 in the Supplement),
317 based on the above analysis. Figure 3a show the trend of observed and reconstructed fine
318 dust concentrations in spring along with three components contributed to the
319 reconstructed trend (i.e., from precipitation, bareness, and surface wind). The
320 reconstructed trend (Reg (all)) largely captures the positive trend in the Southwest shown



321 in the observation (Obs). Among the three factors, precipitation plays the most important
322 role in contributing to the positive trend over the Southwest, consistent with its dominant
323 role in explaining observed interannual variability (Fig. 2b). The increase of fine dust is
324 mainly associated with a decreasing trend of precipitation in the Southwest (Fig. 3b).
325 Such a drying trend has been related to an increase of anticyclonic conditions in the
326 North East Pacific (Prein et al., 2016) and an intensification of Pacific trades during
327 2002-2012 (Delworth et al., 2015).

328 The reconstructed summer trend using coefficients from five-factor regression is
329 very similar to the observation, with a pattern correlation of 0.95 in the domain (Fig. 4a).
330 The positive trend over the central Great Plains is largely contributed by CIN, with a
331 positive center at northern Texas, western Kansas, and Oklahoma. Parts of the positive
332 trend over Oklahoma and western Kansas are contributed by CAPE. In fact, both CIN
333 and CAPE have significant negative trends over the central Great Plains, although the
334 trend of CAPE is slightly weaker than that of CIN (Fig. 4b). A decrease of CIN (i.e., an
335 increase in its absolute value) denotes an increasing inhibition of convection, while a
336 weakening of CAPE denotes a decreasing instability associated with moist convection.
337 Note that CIN is also significantly negatively correlated with fine dust concentration on
338 interannual time scale ($r = -0.39$, $p = 0.05$). This again indicates that CIN plays a more
339 important role than CAPE in the recent positive trend of fine dust.

340 Both the trends of the CIN and CAPE denote an increasing of atmospheric
341 stability. Changes of CIN and CAPE have been related to boundary layer or near-surface
342 temperature and moisture (e.g., Ye et al., 1998; Gettelman et al., 2002; Alappattu and
343 Kunhikrishnan, 2009). Myoung and Nielsen-Gammon (2010b) found that the variations



344 of CIN over Texas in the warm season can be well represented by the differences of
345 temperature at 700 hPa (T_{700}) and surface dew point temperature (T_{dp}), i.e., $T_{700}-T_{dp}$.
346 While T_{700} is a good proxy for temperature at the free-troposphere below the LFC, T_{dp}
347 denotes the dryness at the surface. Thus, $T_{700}-T_{dp}$ represents a joint effect of surface
348 drying and warming at 700 hPa, a generally stable atmosphere. Here we find both CIN
349 and CAPE have significant negative correlations with $T_{700}-T_{dp}$ over the central Great
350 Plains (Fig. 4c). A significant positive trend of $T_{700}-T_{dp}$ is also found, supporting the
351 assumption that the atmospheric stability is enhanced during the period. Such a changes
352 of stability is largely due to the increase of T_{700} , although surface drying also contributes.

353 CIN is also found to be significantly correlated with rain days (daily precipitation
354 ≥ 1 mm day⁻¹) in summer in Texas (Myoung and Nielsen-Gammon, 2010b). Here a
355 similar positive correlation between CIN and rain days in the central Great Plains in also
356 found from 1990 to 2015 ($r=0.79$, $p<0.001$), suggesting that CIN could influence fine
357 dust concentration via its connection with rain days. A stable atmosphere prevents deep
358 moist convection, which reduces the chance of scavenging by precipitation, and also
359 likely prevents dilution of fine dust concentration in the boundary layer with the clean air
360 above through convective mixing. The connection underlying CIN and fine dust
361 concentration is further discussed in section 3.3 using daily data.

362

363 **3.2 The connection between the Great Plains low-level jet and summertime fine dust** 364 **variations in the central Great Plains (CGP)**

365 An important feature related to the moisture and heat transport and precipitation
366 in the Great Plains from late spring to summer is the Great Plains low-level jet (LLJ),



367 which develops in April and reaches its maximum wind speed in June and July at around
368 900 hPa (e.g., Weaver and Nigam, 2008; Pu et al., 2016). The southerly jet covers most of
369 the southern to central Great Plains, and turns into a westerly around 40° N passing
370 through the Midwest. How this jet may influence the dust concentration in the CPG in
371 summer is examined here.

372 Figure 5a shows the time series of the jet index in summer following the
373 definition of Weaver and Nigam (2008) by averaging 900 hPa meridional wind speed at
374 the jet core (25°-35°N, 97°-102°W) from 1990 to 2015. The jet index is significantly
375 positively correlated with fine dust concentration in the CGP ($r=0.56$, $p<0.01$) and also
376 has a significant positive trend in summer, suggesting that the jet also contributes to the
377 increasing of fine dust in the CGP. Such a positive connection between the jet and fine
378 dust concentration can be explained by jet's negative correlation with CIN and positive
379 correlation with the near surface wind speed in the CGP (Figs. 5b). An intensified jet
380 increases the near surface wind speed and meanwhile increases the stability of
381 atmosphere over the CGP by advecting moisture away to the Midwest and increasing
382 local temperature via northward warm temperature advection (e.g., Walters and Winkler,
383 2001; Song et al., 2005; Zhu and Liang, 2013).

384 Because most of the IMPROVE sites (4 out of 6) in the central Great Plains only
385 have records since 2002, correlations between the jet index and fine dust concentration,
386 CIN, and surface wind for 2002-2015 are also calculated (Fig. 5c). The patterns are
387 similar to those during 1990-2015.

388 Dust from Africa can be transported to the southeastern U.S. and even Texas in
389 summer (e.g., Perry et al., 1997; Prospero, 1999a, b; 2010; 2014; Bozlake et al., 2013).



390 Does African dust also contribute to the positive trend of fine dust in the CGP via the jet?
391 Fully addressing this question will require a dust model that can well reproduce the
392 emission and transport processes of African dust, which is beyond the scope of this paper.
393 Here we discuss this question based on observational analysis. The regression and trend
394 analysis above suggests that local atmospheric stability largely contributes to the positive
395 trend. Since African dust is transported to the continental U.S. passing through the
396 Caribbean Sea and the Gulf of Mexico, we assume that the variations of fine dust in
397 stations nearby would reveal the influence of African dust. Two of such stations, VIIS1
398 (18.3°N, 64.8°W) in the Virgin Islands National Park and EVER1 (25.4°N, 80.7°W) in
399 the Everglades National Park, are used. It is found that the records from these stations
400 have significantly positive correlations with fine dust concentration over the southeastern
401 U.S. in JJA, but not over the CGP (Fig. S8 in the Supplement). This suggests that the
402 influence of African dust is largely over the Southeast on seasonal mean, consistent with
403 the results of Hand et al. (2017), who found the influence of North African dust are
404 mainly over the Southeast, Appalachia, and Virgin islands regions in summer as indicated
405 by a shift of elemental composition in IMPROVE sites.

406

407 **3.3 Factors contributing to high dust concentration over the CGP in summer**

408 While the negative correlation between fine dust concentration and precipitation
409 in the Southwest is straightforward, the correlation between fine dust and CIN in the CGP
410 is less obvious. Here we further examine the connection between fine dust and CIN and
411 other factors associated with high dust concentration in the area using daily events. As



412 mentioned earlier, since most stations in the CGP have records since 2002, the following
413 analysis focuses on summer during 2002-2015.

414

415 **3.3.1 Connection between fine dust concentration and CIN**

416 Figures 6a-c show the scatter plot of standardized (means are removed and then
417 divided by one standard deviation) CIN and friction velocity (U^*) anomalies, for all the
418 days in summer from 2002 to 2015, days when IMPROVE records are available (431
419 days), and dusty days, defined as days when daily anomaly of IMPROVE observation is
420 greater than one standard deviation (52 days), respectively. U^* is defined as the
421 following,

$$422 \quad U^* = ([\tau/\rho])^{1/2} = [(\overline{u'w'})^2 + (\overline{v'w'})^2]^{1/4}, \quad (4)$$

423 where τ is the Reynolds stress and ρ is air density, and $\overline{u'w'}$ and $\overline{v'w'}$ are vertical flux of
424 horizontal momentum. We calculated U^* using the surface turbulence stresses ($-\rho\overline{u'w'}$,
425 $-\rho\overline{v'w'}$) from the ERA-Interim. U^* has long been related to dust emission (e.g., Gillette
426 and Passi, 1988; Marticorena and Bergametti, 1995; Zender et al., 2003). As shown in Fig.
427 6, CIN is significantly negatively related to the friction velocity, which is associated with
428 turbulent fluctuations in the boundary layer. This indicates a large negative CIN, or great
429 inhibition for convection, is related to stronger near surface turbulence fluxes and U^* .
430 Such a negative connection is robust both in days with fine dust records and in dusty
431 days. CIN represents the integrated inhibition from the surface to LFC (Eq. 2), then how
432 does CIN relate to surface turbulence fluxes and U^* ?

433 In the CGP, CIN is significantly negatively correlated with near surface
434 temperature, T_{2m} , i.e., a strong inhibition is associated with higher T_{2m} , for all days in JJA



435 and for days when fine dust records are available (Table 1). This is consistent with
436 previous study over Texas (Myoung and Nielsen-Gammon, 2010b). Meanwhile, U^* is
437 significantly positively correlated with T_{2m} (Table 1), indicating that CIN is connected
438 with U^* via its connection with near surface temperature. Also, note such a connection
439 seems not valid during dusty days (correlation between T_{2m} and U^* is not significant).
440 Similarly, we found a close connection among CIN, $T_{700}-T_{dp}$, and U^* (Table 1). This
441 again, suggests that CIN can influence U^* via its connection with surface variables such
442 as temperature and dryness. Variables in Table 1 are all from the ERA-Interim (except
443 CIN) to be consistent with U^* , results are similar if using NARR variables.

444 One hypothesis for the connection between CIN and U^* for dusty days is shown in
445 Table 2. A significant positive correlation between CIN and vertical wind at 850 hPa
446 (w_{850}) is found, indicating that when the inhibition is strong, it favors subsidence. This is
447 consistent with the finding by Riemann-Campe et al. (2009) who found in climatology
448 high CIN value is located over subtropical regions with strong subsidence. The
449 subsidence may transports momentum downward and promotes U^* . This is consistent
450 with the negative correlation between U^* and w_{850} (Table 2). However, we also notice
451 that the above connections in dusty days are not valid in the NARR, suggesting further
452 investigation on this mechanism is needed.

453 Despite the connection between CIN and surface variables, the possible
454 mechanism that strong inhibition prevents dilution is also examined. We found four
455 examples in CALIOP snapshots over the CGP when the daily anomaly of near surface
456 fine dust concentration from the IMPROVE network is greater than one standard
457 deviation. Figure 7 shows nighttime 532 nm total attenuated backscatter (shading) on



458 August 10th, 2007 (top) and on June 21st, 2013 (bottom). Black contours show area with
459 depolarization ratio ≥ 0.2 , denoting dust aerosols. In both cases, the inhibition is quite
460 strong, with CIN anomaly greater than one standard deviation. The difference between
461 the two cases is that on June 21st, 2013, CAPE is higher, which leads to some convection
462 as denoted by the clouds above. However, in both cases, with strong inhibition, dust
463 particles are largely located in a layer between the surface and 2 km. Figure 8 shows a
464 different situation when CIN has positive anomaly (i.e., weak inhibition). In these cases,
465 dust particle extends up to 4 km, and surface fine dust concentrations in the CGP (with
466 anomalies of 2.3 and 2.1 $\mu\text{g m}^{-3}$) are also lower than those in Fig. 7 (with anomalies of
467 4.0 and 7.1 $\mu\text{g m}^{-3}$). Nonetheless, more cases are needed to further verify this mechanism.
468

469 3.3.2 Large-scale circulation pattern in dusty days

470 Figure 9 shows the daily composites of related metrological variables in dusty
471 days, i.e., when daily anomaly of CGP fine dust concentration is greater than one
472 standard deviation. Anomalous high fine dust concentration is associated with a reduced
473 CIN (Fig. 9b) in the CGP, but not so much with CAPE (Fig. 9c). CAPE is anomalously
474 enhanced over the northern Plains and the Midwest. Both the LLJ, near surface wind, and
475 friction velocity are enhanced (Figs. 9d-f). Precipitation (mostly convective precipitation)
476 in the CGP also decreases with reduced cloud cover, but increases in the north (Figs. 9g-
477 i), consistent with enhanced CAPE there. These features are quite consistent with our
478 analysis above on the favorable condition of enhanced fine dust in the CGP.

479 Figure 10 shows the composites of vertical velocity (shading), vertical and
480 meridional wind vectors, specific humidity (purple contours), and potential temperature



481 (grey contours) zonally averaged over the central Great Plains (95° - 102° W), along with
482 fine dust concentration (orange line). Anomalous dry subsidence is centered at 30° - 36° N,
483 with anomalous southerly winds at low-level associated with an intensified jet, while a
484 rising motion of moist air is located around 38 - 42° N with a maximum at 700-400 hPa.
485 The dipole pattern of anomalous vertical velocity is consistent with the precipitation
486 anomaly in the area (Figs. 9g-h). The anomalous potential temperature contour is quite
487 uniform near the surface at 30° - 36° N with an inversion around 700 hPa, indicating a
488 well-mixed boundary layer in the region with increased fine dust.

489 What causes the changes of atmospheric stability, precipitation, and winds?
490 Figure 11 shows the composites of T_{2m} and geopotential height and winds at 850 hPa
491 during dusty days. Following Li et al. (2012a), 1560 gpm contour is used here to denote
492 the western edge of the North Atlantic subtropical high in the 2002-2015 climatology
493 (blue) and in dusty days (red). A westward extension of the subtropical high during dust
494 days is quite evident, with enhanced geopotential height over the southeastern U.S. and
495 the Gulf of Mexico (Fig. 11b). Such a westward extension of the subtropical high
496 intensifies the LLJ by increasing the zonal pressure gradient, and also contributes to the
497 anomalous precipitation and vertical velocity patterns, as similar patterns are found in
498 previous studies associated with a westward extension of the subtropical high (e.g., Li et
499 al., 2012a; their Figs. 3a and 4a). The formation of the North Atlantic subtropical high
500 has been related to the land-sea heating contrast (Wu and Liu, 2003; Liu et al.,
501 2004; Miyasaka and Nakamura, 2005; Li et al., 2012a; Li et al., 2012b). One possible
502 reason of the westward extension of the subtropical high is the anomalous surface



503 warming over large part of the central and eastern U.S. (Fig. 11a) in dusty days that
504 enhances the land-sea temperature gradient.

505

506 **4. Conclusions**

507 Fine dust is an important component in the total PM 2.5 mass in the western to
508 central U.S. in spring and summer (Hand et al. 2017). Previous studies found positive
509 trends of fine dust concentration in the southwestern U.S. in spring and the central U.S. in
510 summer in the past 20 years (Hand et al., 2016;2017;Zhang et al., 2017), but the
511 underlying causes are not clear, especially for the positive trend over the central U.S.
512 This study examined local controlling factors associated with variations of fine dust
513 concentration from Interagency Monitoring of Protected Visual Environments
514 (IMPROVE) stations for 1990-2015 in each season. While precipitation, surface
515 bareness, and wind speed largely control the variation of fine dust concentration in the
516 southwestern U.S., including two convective parameters, convective inhibition (CIN) and
517 convective available potential energy (CAPE) better explains the variations over the
518 Great Plains from spring to fall. In particular, we found that the increasing trend of fine
519 dust concentration over the Southwest in spring is associated with a significantly
520 decreasing trend of precipitation, while the positive trend of fine dust over the central
521 Great Plains (CGP) is largely due to enhanced atmospheric stability revealed by an
522 enhancing of CIN (greater inhibition) and a decreasing of CAPE. Such a stability change
523 is associated with surface drying and warming in the lower troposphere around 700 hPa,
524 i.e., a positive trend of $T_{700}-T_{dp}$. A stable atmosphere prevents moist convection that can
525 remove fine dust by in-cloud or precipitation scavenging and also likely prevent the



526 dilution of fine dust concentration by prohibiting convective mixing between the dusty
527 boundary layer air and the clean air above.

528 The variations of the fine dust concentration in the CGP are also significantly
529 correlated to the Great Plains low-level jet, with a stronger jet corresponding to higher
530 fine dust concentration. Such a connection is largely due to jet's positive correlation with
531 surface wind speed and negative correlation with CIN.

532 The influence of CIN on dust emission is examined using daily data in summer. It
533 is found that CIN is significantly negatively related to surface friction velocity (U^*), i.e.,
534 with greater inhibition in association with stronger U^* . Such a connection is largely due
535 to CIN's connection with surface variables such as 2m temperature and dew point
536 temperature. During dusty days, another possible connection is that the anomalous
537 subsidence associated with strong inhibition may transport momentum downward and
538 increase surface U^* .

539 Dusty days in the CGP in summer are associated with a westward extension of the
540 North Atlantic subtropical high that intensifies the Great Plains low-level jet and surface
541 wind speed, increases atmospheric stability, and also creates anomalous subsidence over
542 the southern to central Great Plains and the Southeast and rising motion over the
543 Midwest, and correspondingly a south-north dipole pattern of precipitation anomaly. The
544 westward extension of the subtropical high is likely associated with the anomalous
545 surface warming over the central to eastern U.S.

546 Our findings have important implications for future projections of fine dust
547 variation in the U.S. Climate models have projected drying trends over the southwestern
548 and the central U.S. (e.g., Seager et al., 2007; Cook et al., 2015) as well as an



549 intensification of the North Atlantic subtropical high (Li et al., 2012b) in the late 21st
550 century, all favorable to an increase of fine dust in the Southwest and central Great
551 Plains. Whether current increasing trends of fine dust will persist into the future requires
552 further investigations that include factors not discussed here such as changes of
553 anthropogenic land use, local synoptic-scale systems (e.g., cyclones and fronts), and
554 remote forcings.

555

556

557

558

559

560

561

562

563

564

565

566

567

568

569

570

571

572 *Acknowledgements.*

573 IMPROVE is a collaborative association of state, tribal, and federal agencies, and
574 international partners. US Environmental Protection Agency is the primary funding
575 source, with contracting and research support from the National Park Service. The Air
576 Quality Group at the University of California, Davis is the central analytical laboratory,
577 with ion analysis provided by Research Triangle Institute, and carbon analysis provided
578 by Desert Research Institute. IMPROVE fine dust data is downloaded from
579 <http://views.cira.colostate.edu/fed/DataWizard/>. AVHRR leaf area index data are
580 available at: <ftp://eclipse.ncdc.noaa.gov/pub/cdr/lai-fapar/files/>. PRECL Precipitation
581 data are provided by the NOAA/OAR/ESRL PSD, Boulder, Colorado, USA, from their
582 web site at <http://www.esrl.noaa.gov/psd/>. The CALIPSO products are downloaded from
583 https://www-calipso.larc.nasa.gov/tools/data_avail/dpo_read.php?y=2007&m=08&d=10.
584 The NCEP/NCAR reanalysis product is obtained from
585 <http://www.esrl.noaa.gov/psd/data/gridded/data.ncep.reanalysis.html> and the ERA-
586 Interim is downloaded from [http://www.ecmwf.int/en/research/climate-reanalysis/era-](http://www.ecmwf.int/en/research/climate-reanalysis/era-interim)
587 interim. The NARR reanalysis is downloaded from
588 <https://www.esrl.noaa.gov/psd/data/gridded/data.narr.html>. This research is supported by
589 NOAA and Princeton University's Cooperative Institute for Climate Science and NASA
590 under grant NNH14ZDA001N-ACMAP. The authors thank Drs. Stuart Evans and Jordan
591 Schnell for their helpful comments on the early version of this paper.

592

593

594



- 595
596
597
598
599
600
601
602
603
604
605
606
607
608
609
610
611
612
613
614
615
616
617
618
- References
- Abudu, S., Cui, C. L., King, J. P., Moreno, J., and Bawazir, A. S.: Modeling of daily pan evaporation using partial least squares regression, *Sci China Technol Sc*, 54, 163-174, [10.1007/s11431-010-4205-z](https://doi.org/10.1007/s11431-010-4205-z), 2011.
- Alappattu, D. P., and Kunhikrishnan, P. K.: Premonsoon estimates of convective available potential energy over the oceanic region surrounding the Indian subcontinent, *J Geophys Res-Atmos*, 114, [10.1029/2008jd011521](https://doi.org/10.1029/2008jd011521), 2009.
- Bozlaker, A., Prospero, J. M., Fraser, M. P., and Chellam, S.: Quantifying the Contribution of Long-Range Saharan Dust Transport on Particulate Matter Concentrations in Houston, Texas, Using Detailed Elemental Analysis, *Environ Sci Technol*, 47, 10179-10187, [10.1021/es4015663](https://doi.org/10.1021/es4015663), 2013.
- Chen, M. Y., Xie, P. P., Janowiak, J. E., and Arkin, P. A.: Global land precipitation: A 50-yr monthly analysis based on gauge observations, *J Hydrometeorol*, 3, 249-266, [Doi 10.1175/1525-7541\(2002\)003<0249:Glpaym>2.0.Co;2](https://doi.org/10.1175/1525-7541(2002)003<0249:Glpaym>2.0.Co;2), 2002.
- Claverie, M., Vermote, E., and NOAA-CDR-Program: NOAA Climate Data Record (CDR) of Leaf Area Index (LAI) and Fraction of Absorbed Photosynthetically Active Radiation (FAPAR), Version 4, NOAA National Climatic Data Center, [10.7289/V5M043BX](https://doi.org/10.7289/V5M043BX), 2014.
- Claverie, M., Matthews, J. L., Vermote, E. F., and Justice, C. O.: A 30+ Year AVHRR LAI and FAPAR Climate Data Record: Algorithm Description and Validation, *Remote Sens-Basel*, 8, [10.3390/rs8030263](https://doi.org/10.3390/rs8030263), 2016.
- Colby, F. P.: Convective Inhibition as a Predictor of Convection during Ave-Sesame-Ii, *Mon Weather Rev*, 112, 2239-2252, [Doi 10.1175/1520-0493\(1984\)112<2239:Ciaapo>2.0.Co;2](https://doi.org/10.1175/1520-0493(1984)112<2239:Ciaapo>2.0.Co;2), 1984.



- 619 Cook, B. I., Ault, T. R., and Smerdon, J. E.: Unprecedented 21st century drought risk in
620 the American Southwest and Central Plains, *Science Advances*, 1, 1-7,
621 10.1126/sciadv.1400082 2015.
- 622 Creamean, J. M., Spackman, J. R., Davis, S. M., and White, A. B.: Climatology of long-
623 range transported Asian dust along the West Coast of the United States, *J*
624 *Geophys Res-Atmos*, 119, 12171-12185, 10.1002/2014jd021694, 2014.
- 625 Crooks, J. L., Cascio, W. E., Percy, M. S., Reyes, J., Neas, L. M., and Hilborn, E. D.: The
626 Association between Dust Storms and Daily Non-Accidental Mortality in the
627 United States, 1993-2005, *Environ Health Persp*, 124, 1735-1743,
628 10.1289/Ehp216, 2016.
- 629 Cuesta, J., Marsham, J. H., Parker, D. J., and Flamant, C.: Dynamical mechanisms
630 controlling the vertical redistribution of dust and the thermodynamic structure of
631 the West Saharan atmospheric boundary layer during summer, *Atmos Sci Lett*,
632 10, 34-42, 10.1002/asl.207, 2009.
- 633 Dee, D. P., Uppala, S. M., Simmons, A. J., Berrisford, P., Poli, P., Kobayashi, S., Andrae,
634 U., Balmaseda, M. A., Balsamo, G., Bauer, P., Bechtold, P., Beljaars, A. C. M.,
635 van de Berg, L., Bidlot, J., Bormann, N., Delsol, C., Dragani, R., Fuentes, M.,
636 Geer, A. J., Haimberger, L., Healy, S. B., Hersbach, H., Holm, E. V., Isaksen, L.,
637 Kallberg, P., Kohler, M., Matricardi, M., McNally, A. P., Monge-Sanz, B. M.,
638 Morcrette, J. J., Park, B. K., Peubey, C., de Rosnay, P., Tavolato, C., Thepaut, J.
639 N., and Vitart, F.: The ERA-Interim reanalysis: configuration and performance of
640 the data assimilation system, *Q J Roy Meteor Soc*, 137, 553-597, 10.1002/qj.828,
641 2011.



- 642 Delworth, T. L., Zeng, F. R., Rosati, A., Vecchi, G. A., and Wittenberg, A. T.: A Link
643 between the Hiatus in Global Warming and North American Drought, *J Climate*,
644 28, 3834-3845, 10.1175/Jcli-D-14-00616.1, 2015.
- 645 Duce, R. A.: Sources, distributions, and fluxes of mineral aerosols and their relationship
646 to climate, in: *Dalhem Workshop on Aerosol Forcing of Climate*, edited by:
647 Charlson, R. J., and Heintzenberg, J., John Wiley, New York, 43-72, 1995.
- 648 Fischer, E. V., Hsu, N. C., Jaffe, D. A., Jeong, M. J., and Gong, S. L.: A decade of dust:
649 Asian dust and springtime aerosol load in the US Pacific Northwest, *Geophys Res*
650 *Lett*, 36, 10.1029/2008gl036467, 2009.
- 651 Gettelman, A., Seidel, D. J., Wheeler, M. C., and Ross, R. J.: Multidecadal trends in
652 tropical convective available potential energy, *J Geophys Res-Atmos*, 107,
653 10.1029/2001jd001082, 2002.
- 654 Gillette, D. A., and Passi, R.: Modeling Dust Emission Caused by Wind Erosion, *J*
655 *Geophys Res-Atmos*, 93, 14233-14242, DOI 10.1029/JD093iD11p14233, 1988.
- 656 Ginoux, P., Prospero, J. M., Gill, T. E., Hsu, N. C., and Zhao, M.: Global-Scale
657 Attribution of Anthropogenic and Natural Dust Sources and Their Emission Rates
658 Based on Modis Deep Blue Aerosol Products, *Rev Geophys*, 50,
659 10.1029/2012rg000388, 2012.
- 660 Hand, J. L., Copeland, S. A., Day, D. E., Dillner, A. M., Indresand, H., Malm, W. C.,
661 McDade, C. E., Moore, C. T., Pitchford, M. L., Schichtel, B. A., and Watson, J.
662 G.: IMPROVE (Interagency Monitoring of Protected Visual Environments):
663 Spatial and seasonal patterns and temporal variability of haze and its constituents
664 in the United States, 2011.



- 665 Hand, J. L., Schichtel, B. A., Pitchford, M., Malm, W. C., and Frank, N. H.: Seasonal
666 composition of remote and urban fine particulate matter in the United States, J
667 Geophys Res-Atmos, 117, 10.1029/2011jd017122, 2012.
- 668 Hand, J. L., White, W. H., Gebhart, K. A., Hyslop, N. P., Gill, T. E., and Schichtel, B. A.:
669 Earlier onset of the spring fine dust season in the southwestern United States,
670 Geophys Res Lett, 43, 4001-4009, 10.1002/2016gl068519, 2016.
- 671 Hand, J. L., Gill, T. E., and Schichtel, B. A.: Spatial and seasonal variability in fine
672 mineral dust and coarse aerosol mass at remote sites across the United States, J
673 Geophys Res-Atmos, 122, 3080-3097, 10.1002/2016jd026290, 2017.
- 674 Helfand, H. M., and Schubert, S. D.: Climatology of the Simulated Great-Plains Low-
675 Level Jet and Its Contribution to the Continental Moisture Budget of the United-
676 States, J Climate, 8, 784-806, Doi 10.1175/1520-
677 0442(1995)008<0784:Cotsgp>2.0.Co;2, 1995.
- 678 Hyslop, N. P., Trzepla, K., and White, W. H.: Assessing the Suitability of Historical
679 PM_{2.5} Element Measurements for Trend Analysis, Environ Sci Technol, 49,
680 9247-9255, 10.1021/acs.est.5b01572, 2015.
- 681 Kok, J. F.: A scaling theory for the size distribution of emitted dust aerosols suggests
682 climate models underestimate the size of the global dust cycle, P Natl Acad Sci
683 USA, 108, 1016-1021, 10.1073/pnas.1014798108, 2011.
- 684 Li, F. Y., Ginoux, P., and Ramaswamy, V.: Transport of Patagonian dust to Antarctica, J
685 Geophys Res-Atmos, 115, 10.1029/2009jd012356, 2010.



- 686 Li, L. F., Li, W. H., and Kushnir, Y.: Variation of the North Atlantic subtropical high
687 western ridge and its implication to Southeastern US summer precipitation, *Clim*
688 *Dynam*, 39, 1401-1412, 10.1007/s00382-011-1214-y, 2012a.
- 689 Li, W. H., Li, L. F., Ting, M. F., and Liu, Y. M.: Intensification of Northern Hemisphere
690 subtropical highs in a warming climate, *Nat Geosci*, 5, 830-834,
691 10.1038/Ngeo1590, 2012b.
- 692 Liu, Y. M., Wu, G. X., and Ren, R. C.: Relationship between the subtropical anticyclone
693 and diabatic heating, *J Climate*, 17, 682-698, Doi 10.1175/1520-
694 0442(2004)017<0682:Rbtsaa>2.0.Co;2, 2004.
- 695 Malm, W. C., Sisler, J. F., Huffman, D., Eldred, R. A., and Cahill, T. A.: Spatial and
696 Seasonal Trends in Particle Concentration and Optical Extinction in the United-
697 States, *J Geophys Res-Atmos*, 99, 1347-1370, Doi 10.1029/93jd02916, 1994.
- 698 Marsham, J. H., Parker, D. J., Grams, C. M., Taylor, C. M., and Haywood, J. M.: Uplift
699 of Saharan dust south of the intertropical discontinuity, *J Geophys Res-Atmos*,
700 113, 10.1029/2008jd009844, 2008.
- 701 Marticorena, B., and Bergametti, G.: Modeling the Atmospheric Dust Cycle .1. Design of
702 a Soil-Derived Dust Emission Scheme, *J Geophys Res-Atmos*, 100, 16415-16430,
703 Doi 10.1029/95jd00690, 1995.
- 704 Mesinger, F., DiMego, G., Kalnay, E., Mitchell, K., Shafran, P. C., Ebisuzaki, W., Jovic,
705 D., Woollen, J., Rogers, E., Berbery, E. H., Ek, M. B., Fan, Y., Grumbine, R.,
706 Higgins, W., Li, H., Lin, Y., Manikin, G., Parrish, D., and Shi, W.: North
707 American regional reanalysis, *B Am Meteorol Soc*, 87, 343-360, 10.1175/Bams-
708 87-3-343, 2006.



- 709 Miyasaka, T., and Nakamura, H.: Structure and formation mechanisms of the northern
710 hemisphere summertime subtropical highs, *J Climate*, 18, 5046-5065, Doi
711 10.1175/Jcli3599.1, 2005.
- 712 Morman, S. A., and Plumlee, G. S.: The role of airborne mineral dusts in human disease,
713 *Aeolian Res*, 9, 203-212, 10.1016/j.aeolia.2012.12.001, 2013.
- 714 Myoung, B., and Nielsen-Gammon, J. W.: Sensitivity of Monthly Convective
715 Precipitation to Environmental Conditions, *J Climate*, 23, 166-188,
716 10.1175/2009jcli2792.1, 2010a.
- 717 Myoung, B., and Nielsen-Gammon, J. W.: The Convective Instability Pathway to Warm
718 Season Drought in Texas. Part I: The Role of Convective Inhibition and Its
719 Modulation by Soil Moisture, *J Climate*, 23, 4461-4473, 10.1175/2010jcli2946.1,
720 2010b.
- 721 O'Brien, R. M.: A caution regarding rules of thumb for variance inflation factors, *Qual*
722 *Quant*, 41, 673-690, 10.1007/s11135-006-9018-6, 2007.
- 723 Perry, K. D., Cahill, T. A., Eldred, R. A., Dutcher, D. D., and Gill, T. E.: Long-range
724 transport of North African dust to the eastern United States, *J Geophys Res-*
725 *Atmos*, 102, 11225-11238, Doi 10.1029/97jd00260, 1997.
- 726 Prein, A. F., Holland, G. J., Rasmussen, R. M., Clark, M. P., and Tye, M. R.: Running
727 dry: The US Southwest's drift into a drier climate state, *Geophys Res Lett*, 43,
728 1272-1279, 10.1002/2015gl066727, 2016.
- 729 Prospero, J. M.: Long-term measurements of the transport of African mineral dust to the
730 southeastern United States: Implications for regional air quality, *J Geophys Res-*
731 *Atmos*, 104, 15917-15927, Doi 10.1029/1999jd900072, 1999a.



- 732 Prospero, J. M.: Long-range transport of mineral dust in the global atmosphere: Impact of
733 African dust on the environment of the southeastern United States, P Natl Acad
734 Sci USA, 96, 3396-3403, DOI 10.1073/pnas.96.7.3396, 1999b.
- 735 Prospero, J. M., Landing, W. M., and Schulz, M.: African dust deposition to Florida:
736 Temporal and spatial variability and comparisons to models, J Geophys Res-
737 Atmos, 115, 10.1029/2009jd012773, 2010.
- 738 Prospero, J. M., Collard, F. X., Molinie, J., and Jeannot, A.: Characterizing the annual
739 cycle of African dust transport to the Caribbean Basin and South America and its
740 impact on the environment and air quality, Global Biogeochem Cy, 28, 757-773,
741 10.1002/2013gb004802, 2014.
- 742 Pu, B., and Dickinson, R. E.: Diurnal Spatial Variability of Great Plains Summer
743 Precipitation Related to the Dynamics of the Low-Level Jet, J Atmos Sci, 71,
744 1807-1817, 10.1175/Jas-D-13-0243.1, 2014.
- 745 Pu, B., Dickinson, R. E., and Fu, R.: Dynamical connection between Great Plains low-
746 level winds and variability of central Gulf States precipitation, J Geophys Res-
747 Atmos, 121, 3421-3434, 10.1002/2015jd024045, 2016.
- 748 Pu, B., and Ginoux, P.: Projection of American dustiness in the late 21st century due to
749 climate change, Scientific Reports, 7:5553, 1-10, 10.1038/s41598-017-05431-9,
750 2017.
- 751 Reid, J. S., Jonsson, H. H., Maring, H. B., Smirnov, A., Savoie, D. L., Cliff, S. S., Reid,
752 E. A., Livingston, J. M., Meier, M. M., Dubovik, O., and Tsay, S. C.: Comparison
753 of size and morphological measurements of coarse mode dust particles from
754 Africa, J Geophys Res-Atmos, 108, 10.1029/2002jd002485, 2003.



- 755 Riemann-Campe, K., Fraedrich, K., and Lunkeit, F.: Global climatology of Convective
756 Available Potential Energy (CAPE) and Convective Inhibition (CIN) in ERA-40
757 reanalysis, *Atmos Res*, 93, 534-545, [10.1016/j.atmosres.2008.09.037](https://doi.org/10.1016/j.atmosres.2008.09.037), 2009.
- 758 Ruane, A. C.: NARR's Atmospheric Water Cycle Components. Part I: 20-Year Mean and
759 Annual Interactions, *J Hydrometeorol*, 11, 1205-1219, [10.1175/2010jhm1193.1](https://doi.org/10.1175/2010jhm1193.1),
760 2010a.
- 761 Ruane, A. C.: NARR's Atmospheric Water Cycle Components. Part II: Summertime
762 Mean and Diurnal Interactions, *J Hydrometeorol*, 11, 1220-1233,
763 [10.1175/2010jhm1279.1](https://doi.org/10.1175/2010jhm1279.1), 2010b.
- 764 Ruiz-Barradas, A., and Nigam, S.: Great plains hydroclimate variability: The view from
765 North American regional reanalysis, *J Climate*, 19, 3004-3010, Doi
766 [10.1175/Jcli3768.1](https://doi.org/10.1175/Jcli3768.1), 2006.
- 767 Sassen, K.: The Polarization Lidar Technique for Cloud Research - a Review and Current
768 Assessment, *B Am Meteorol Soc*, 72, 1848-1866, Doi [10.1175/1520-
769 0477\(1991\)072<1848:Tpltfc>2.0.Co;2](https://doi.org/10.1175/1520-0477(1991)072<1848:Tpltfc>2.0.Co;2), 1991.
- 770 Seager, R., Ting, M. F., Held, I., Kushnir, Y., Lu, J., Vecchi, G., Huang, H. P., Harnik,
771 N., Leetmaa, A., Lau, N. C., Li, C. H., Velez, J., and Naik, N.: Model projections
772 of an imminent transition to a more arid climate in southwestern North America,
773 *Science*, 316, 1181-1184, [10.1126/science.1139601](https://doi.org/10.1126/science.1139601), 2007.
- 774 Song, J., Liao, K., Coulter, R. L., and Lesht, B. M.: Climatology of the low-level jet at
775 the southern Great Plains atmospheric Boundary Layer Experiments site, *J Appl
776 Meteorol*, 44, 1593-1606, Doi [10.1175/Jam2294.1](https://doi.org/10.1175/Jam2294.1), 2005.



- 777 Sorooshian, A., Wonaschutz, A., Jarjour, E. G., Hashimoto, B. I., Schichtel, B. A., and
778 Betterton, E. A.: An aerosol climatology for a rapidly growing arid region
779 (southern Arizona): Major aerosol species and remotely sensed aerosol properties,
780 J Geophys Res-Atmos, 116, 10.1029/2011jd016197, 2011.
- 781 Tong, D. Q., Wang, J. X. L., Gill, T. E., Lei, H., and Wang, B. Y.: Intensified dust storm
782 activity and Valley fever infection in the southwestern United States, Geophys
783 Res Lett, 44, 4304-4312, 10.1002/2017gl073524, 2017.
- 784 Walters, C. K., and Winkler, J. A.: Airflow configurations of warm season southerly low-
785 level wind maxima in the Great Plains. Part I: spatial and temporal characteristics
786 and relationship to convection, Weather Forecast, 16, 513-530, Doi
787 10.1175/1520-0434(2001)016<0513:Acowss>2.0.Co;2, 2001.
- 788 Weaver, S. J., and Nigam, S.: Variability of the great plains low-level jet: Large-scale
789 circulation context and hydroclimate impacts, J Climate, 21, 1532-1551,
790 10.1175/2007jcli1586.1, 2008.
- 791 Winker, D. M., Hunt, W., and Hostetler, C.: Status and performance of the CALIOP
792 lidar, Bba Lib, 5575, 8-15, 10.1117/12.571955, 2004.
- 793 Winker, D. M., Hunt, W. H., and McGill, M. J.: Initial performance assessment of
794 CALIOP, Geophys Res Lett, 34, 10.1029/2007gl030135, 2007.
- 795 Wu, G. X., and Liu, Y. M.: Summertime quadruplet heating pattern in the subtropics and
796 the associated atmospheric circulation, Geophys Res Lett, 30,
797 10.1029/2002gl016209, 2003.



798 Ye, B., Del Genio, A. D., and Lo, K. K. W.: CAPE variations in the current climate and
799 in a climate change, *J Climate*, 11, 1997-2015, Doi 10.1175/1520-0442-
800 11.8.1997, 1998.

801 Yu, H. B., Remer, L. A., Chin, M., Bian, H. S., Tan, Q., Yuan, T. L., and Zhang, Y.:
802 Aerosols from Overseas Rival Domestic Emissions over North America, *Science*,
803 337, 566-569, 10.1126/science.1217576, 2012.

804 Zender, C. S., Bian, H. S., and Newman, D.: Mineral Dust Entrainment and Deposition
805 (DEAD) model: Description and 1990s dust climatology, *J Geophys Res-Atmos*,
806 108, 10.1029/2002jd002775, 2003.

807 Zhang, L., Henze, D. K., Grell, G. A., Torres, O., Jethva, H., and Lamsal, L. N.: What
808 factors control the trend of increasing AAOD over the United States in the last
809 decade?, *J. Geophys. Res. Atmos*, 122, 1797-1810, 10.1002/2016JD025472,
810 2017.

811 Zhu, J. H., and Liang, X. Z.: Impacts of the Bermuda High on Regional Climate and
812 Ozone over the United States, *J Climate*, 26, 1018-1032, 10.1175/Jcli-D-12-
813 00168.1, 2013.

814

815

816

817



818 Table 1 Correlations between friction velocity (U^*) and CIN, CIN and 2 meter
819 temperature (T_{2m}), T_{2m} and U^* , $T_{700}-T_{dp}$ (the differences between air temperature at 700
820 hPa and 2m dew point temperature) and CIN, $T_{700}-T_{dp}$ and U^* for all days in JJA from
821 2002 to 2015 (1288 days), days when fine dust concentration is available (431 days), and
822 dusty days (52 days). All values are significant at the 95% confidence level (t-test) except
823 those listed in italic.

824

825 Table 2 Correlations between U^* and CIN, CIN and vertical wind speed at 850 hPa
826 (w_{850}), w_{850} and U^* during dusty days in JJA from 2002 to 2015. All values are
827 significant at the 95% confidence level except the value significant at the 90% confidence
828 level is labeled with a “+” (t-test).

829

830

831

832

833

834

835

836

837

838

839

840



841 Figure 1. Trend (shading) of fine dust concentration ($\mu\text{g m}^{-3}$) from 1990 to 2015 in (a)
842 DJF, (b) MAM, (c) JJA, and (d) SON from IMPROVE gridded data. Dotted areas are
843 significant at the 95% confidence level. The colored circles show the trend at IMPROVE
844 stations with consecutive records for at least 23 years during 1990-2015. Circles with
845 green outlines denote that the trend is significant at the 90% confidence level. Black
846 boxes denote the averaging areas of the southwestern U.S. (left) and the Great Plains
847 (right).

848

849 Figure 2. (a)-(d) Multiple linear regression coefficients calculated by regressing fine dust
850 concentration from 1990-2015 onto standardized precipitation (purple), bareness
851 (orange), and surface wind (green). Color denotes the most influential factor at each grid
852 (i.e., the largest regression coefficient in absolute value among the three), while
853 saturation of the color shows the magnitude of the coefficient (0 to 0.3). Areas significant
854 at the 95% confidence levels are dotted. (e) Bar-plot showing the correlations between
855 observed regional mean fine dust concentration and the reconstructed concentration using
856 3, 4, and 5 controlling factors (light, median, and deep blue), and pattern correlation
857 between trends from the observation and from reconstructed fine dust using 3, 4, and 5
858 factors (light, medium, and deep pink) in the Great Plains (GP) and the southwestern U.S.
859 (WST, black boxes in Fig. 1). “3-factor” denotes precipitation, bareness, and surface
860 wind, “4-factor” denotes precipitation, bareness, surface wind, and CIN, “5-factor”
861 denotes precipitation, bareness, surface wind, CIN, and CAPE.

862



863 Figure 3. (a) Observed (Obs) and reconstructed (Reg) trends of fine dust concentration
864 ($\mu\text{g m}^{-3}$) using three factors in spring from 1990 to 2015. The contributions from each
865 factor (precipitation, bareness, and surface wind) to the overall reconstructed trend are
866 also shown (second row). Dotted areas are significant at the 90% confidence level.
867 Pattern correlation between reconstructed dust concentration trends and observed trends
868 are shown at the top right corner of each plot. Black box denotes the southwestern U.S.
869 (WST). (b) Time series of fine dust concentration (cyan) and precipitation (purple)
870 averaged over the WST and their linear trends (dashed lines; values are listed at bottom
871 left) in spring from 1990 to 2015. Gray shading denotes \pm one standard error of the
872 observations. The correlation between fine dust and precipitation is also listed at the
873 bottom in purple.

874

875 Figure 4. (a) Observed (Obs) and reconstructed (Reg) trends of fine dust concentration (μg
876 m^{-3}) using five factors in summer from 1990-2015. The contributions from each factor
877 (precipitation, bareness, surface wind, CAPE, and CIN) are also shown (second and third
878 rows). Dotted areas are significant at the 90% confidence level. Pattern correlation
879 between reconstructed dust concentration trends and the observed trends are shown at the
880 right corner of each plot. Black box denotes the central Great Plains (CGP). (b) Time
881 series of fine dust concentration (cyan), CIN (orange), and CAPE (deep blue) averaged
882 over the CGP and their linear trends (dashed lines). Gray shading denotes \pm one standard
883 error of the observations. (c) Time series of $T_{700}-T_{dp}$ (black), T_{700} (green) and T_{dp} (light
884 blue) and their linear trends (dashed lines) in summer from 1990 to 2015.

885



886 Figure 5. (a) Time series of fine dust concentration ($\mu\text{g m}^{-3}$) averaged in the CGP (cyan)
887 and the index of the Great Plains low-level jet (magenta) and their trends (dashed line) in
888 JJA from 1990 to 2015. Gray shading denotes \pm one standard error of the observations.
889 Correlations between the jet index and fine dust concentration, CIN, and near surface
890 wind speed for (b) 1990-2015 and (c) 2002-2015. Colored circles denotes correlations at
891 IMPROVE stations, with green outlines denotes the correlation is significant at the 90%
892 confidence level. Areas significant at the 95% confidence level are dotted in (b) and
893 significant at the 90% confidence level are dotted in (c).

894

895 Figure 6. Scatter plot of standardized friction velocity (U^*) and CIN anomalies for (a) all
896 days in JJA from 2002-2015, (b) days when fine dust data is available, and (c) dusty days
897 (when daily fine dust concentration anomaly is greater than one standard deviation).

898

899 Figure 7. Nighttime 532 nm total attenuated backscatter (shading) and depolarization
900 ratio (black contours, values ≥ 0.2 are shown) from CALIOP on August 10th, 2007 (top
901 left) and on June 21st, 2013 (bottom left), along with fine dust concentration anomaly (μg
902 m^{-3} ; shading, right column) and CIN anomaly (blue contour, only negative values from -
903 60 to -120 J kg^{-1} are shown). CALIOP orbit tracks are shown in grey lines (right column)
904 with cyan part and sampling points (A-F) denote the cross-section shown on the left
905 column.

906

907 Figure 8. Same as Fig. 10 but for July 2nd, 2011 (top) and July 2nd, 2012 (bottom). Only
908 positive CIN anomalies from 25 to 50 J kg^{-1} are shown (light purple contour).



909 Figure 9. Daily composites of the anomalies of (a) fine dust concentration ($\mu\text{g m}^{-3}$), (b)
910 CIN (J kg^{-1}), (c) CAPE (J kg^{-1}), (d) 900 hPa wind speed (m s^{-1}), (e) 10 m wind speed (m
911 s^{-1}), (f) U^* (m s^{-1}), (g) total precipitation (mm day^{-1}), (h) convective precipitation (mm
912 day^{-1}), and (i) total cloud cover (%) during dusty days in JJA from 2002 to 2015. Dotted
913 areas are significant at the 95% confidence level. 900 hPa and 10 m wind anomalies
914 (green vectors) significant at the 95% confidence level are shown in (d) and (e).

915

916 Figure 10. Daily composite of vertical velocity (shading; 10^{-2} m s^{-1}), potential
917 temperature (grey contours; K), and specific humidity (purple contours; g kg^{-1}) from the
918 ERA-Interim, and fine dust concentration anomalies (bottom; orange line) averaged
919 between 95° and 102° W for dusty days in JJA from 2002 to 2015. Topography is
920 masked out in grey. Cyan lines denote the domain of the CGP.

921

922 Figure 11. Daily composites of (a) $T_{2\text{m}}$ (K) and (b) 850 hPa geopotential height (gpm)
923 and horizontal wind vectors (m s^{-1} ; grey) from the ERA-Interim averaged over dusty days
924 in JJA from 2002-2015. Blue and red contours denote 1560 geopotential height in the
925 climatology (2002-2015) and during dusty days, respectively. Areas significant at the
926 95% confidence level are dotted. Wind vectors significant at the 95% confidence level
927 are plotted in green.

928

929

930

931



932 Table 1 Correlations between friction velocity (U^*) and CIN, CIN and 2 meter
933 temperature (T_{2m}), T_{2m} and U^* , $T_{700}-T_{dp}$ (the differences between air temperature at 700
934 hPa and 2m dew point temperature) and CIN, $T_{700}-T_{dp}$ and U^* for all days in JJA from
935 2002 to 2015 (1288 days), days when fine dust concentration is available (431 days), and
936 dusty days (52 days). All values are significant at the 95% confidence level (t-test) except
937 those listed in italic.
938

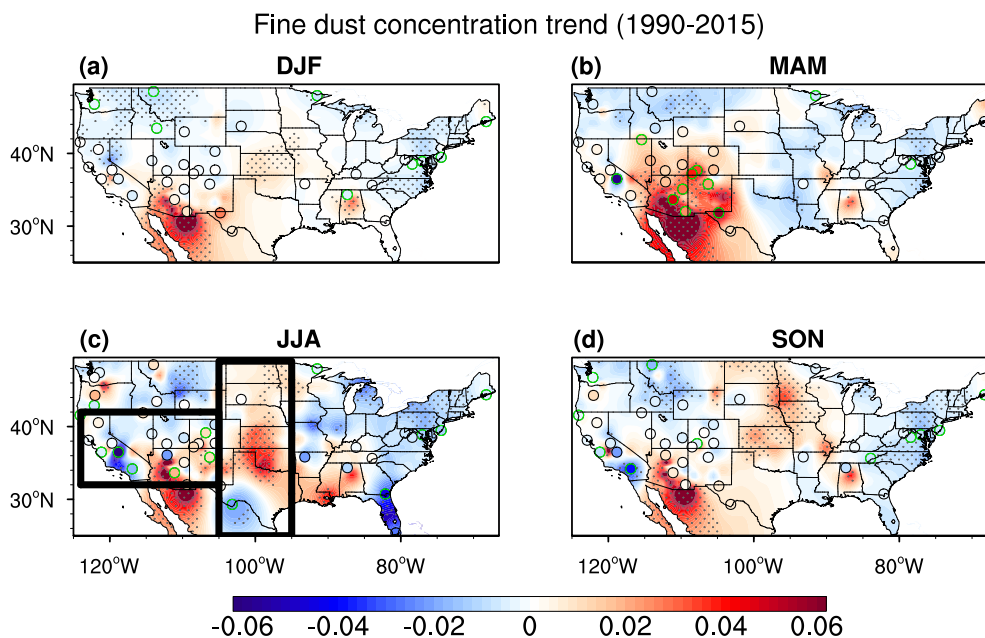
Variables	All days in JJA	Available days	Dusty days
U^* , CIN	-0.54	-0.54	-0.44
CIN, T_{2m}	-0.59	-0.59	-0.39
T_{2m} , U^*	0.39	0.37	<i>0.19</i>
CIN, $T_{700}-T_{dp}$	-0.59	-0.62	-0.59
$T_{700}-T_{dp}$, U^*	0.37	0.38	<i>0.14</i>

939
940
941
942
943
944
945
946
947

Table 2 Correlations between U^* and CIN, CIN and vertical wind speed at 850 hPa
(w_{850}), w_{850} and U^* during dusty days in JJA from 2002 to 2015. All values are
significant at the 95% confidence level except the value significant at the 90% confidence
level is labeled with a “+” (t-test).

Variables	Dusty days
U^* , CIN	-0.44
CIN, w_{850}	0.28 ⁺
w_{850} , U^*	-0.32

948
949
950
951
952
953
954
955
956
957
958
959
960
961
962
963
964
965
966
967



968

969

970 Figure 1. Trend (shading) of fine dust concentration ($\mu\text{g m}^{-3}$) from 1990 to 2015 in (a)

971 DJF, (b) MAM, (c) JJA, and (d) SON from IMPROVE gridded data. Dotted areas are

972 significant at the 95% confidence level. The colored circles show the trend at IMPROVE

973 stations with consecutive records for at least 23 years during 1990-2015. Circles with

974 green outlines denote that the trend is significant at the 90% confidence level. Black

975 boxes denote the averaging areas of the southwestern U.S. (left) and the Great Plains

976 (right).

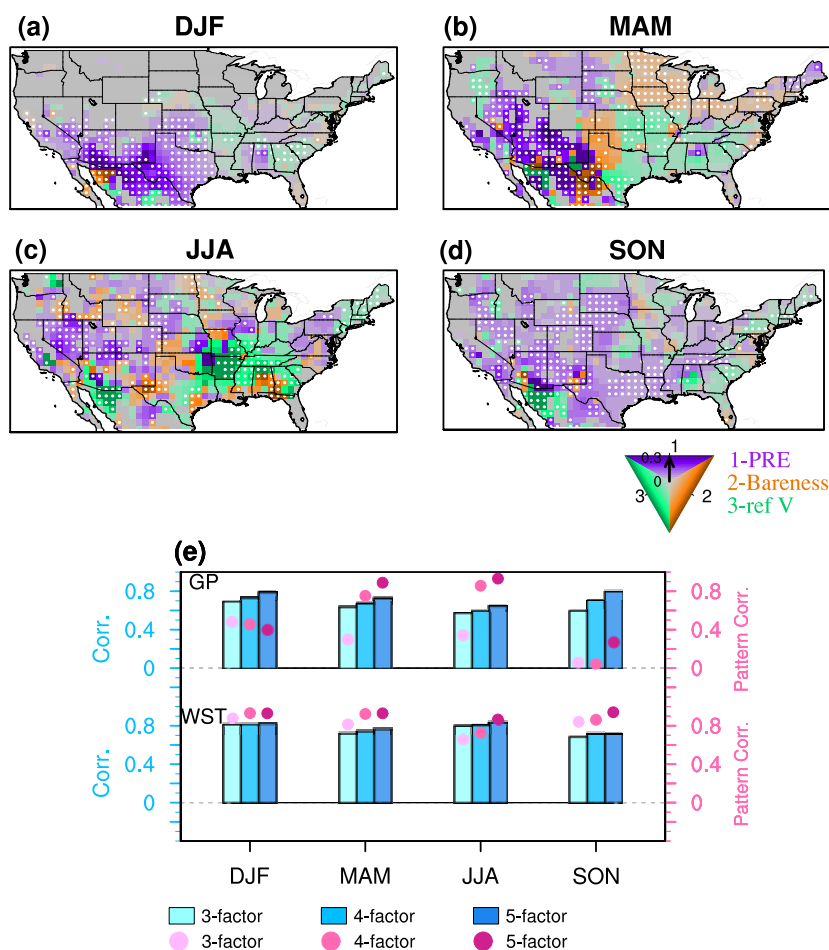
977

978

979

980

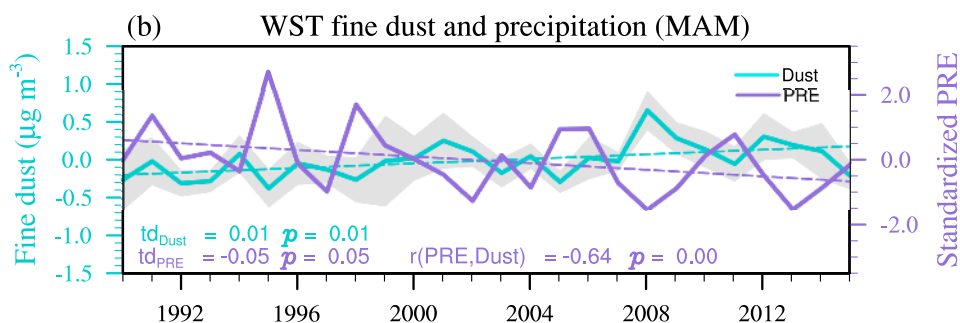
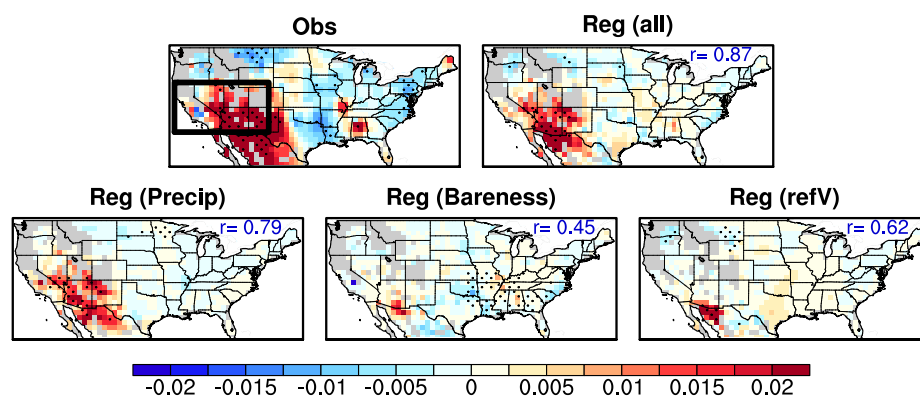
981



982
 983 Figure 2. (a)-(d) Multiple linear regression coefficients calculated by regressing fine dust
 984 concentration from 1990–2015 onto standardized precipitation (purple), bareness
 985 (orange), and surface wind (green). Color denotes the most influential factor at each grid
 986 (i.e., the largest regression coefficient in absolute value among the three), while
 987 saturation of the color shows the magnitude of the coefficient (0 to 0.3). Areas significant
 988 at the 95% confidence levels are dotted. (e) Bar-plot showing the correlations between
 989 observed regional mean fine dust concentration and the reconstructed concentration using
 990 3, 4, and 5 controlling factors (light, median, and deep blue), and pattern correlation
 991 between trends from the observation and from reconstructed fine dust using 3, 4, and 5
 992 factors (light, medium, and deep pink) in the Great Plains (GP) and the southwestern U.S.
 993 (WST, black boxes in Fig. 1). “3-factor” denotes precipitation, bareness, and surface
 994 wind, “4-factor” denotes precipitation, bareness, surface wind, and CIN, “5-factor”
 995 denotes precipitation, bareness, surface wind, CIN, and CAPE.
 996
 997



(a) Obs and Reg fine dust trend (1990-2015 MAM)

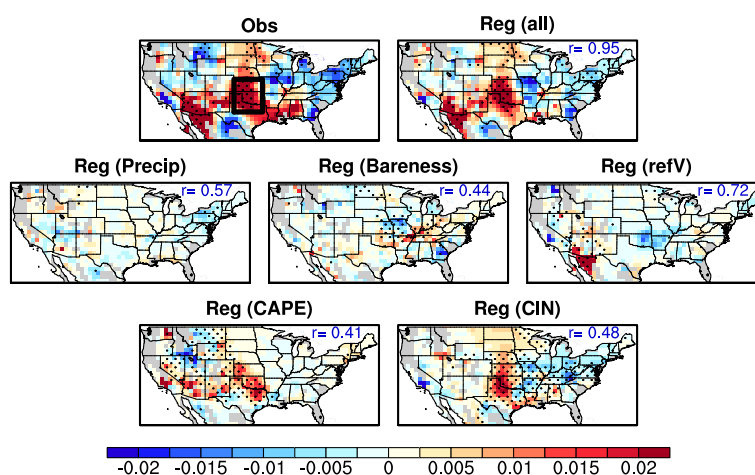


998
 999
 1000
 1001
 1002
 1003
 1004
 1005
 1006
 1007
 1008
 1009
 1010
 1011
 1012
 1013
 1014
 1015
 1016
 1017

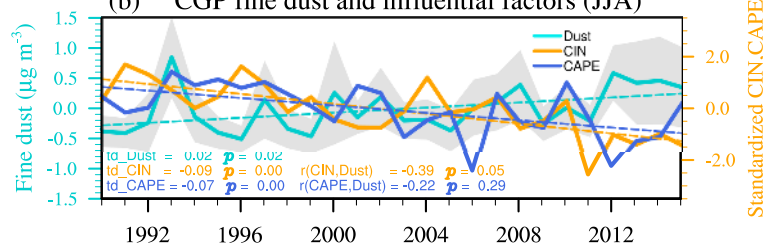
Figure 3. (a) Observed (Obs) and reconstructed (Reg) trends of fine dust concentration ($\mu\text{g m}^{-3}$) using three factors in spring from 1990 to 2015. The contributions from each factor (precipitation, bareness, and surface wind) to the overall reconstructed trend are also shown (second row). Dotted areas are significant at the 90% confidence level. Pattern correlation between reconstructed dust concentration trends and observed trends are shown at the top right corner of each plot. Black box denotes the southwestern U.S. (WST). (b) Time series of fine dust concentration (cyan) and precipitation (purple) averaged over the WST and their linear trends (dashed lines; values are listed at bottom left) in spring from 1990 to 2015. Gray shading denotes \pm one standard error of the observations. The correlation between fine dust and precipitation is also listed at the bottom in purple.



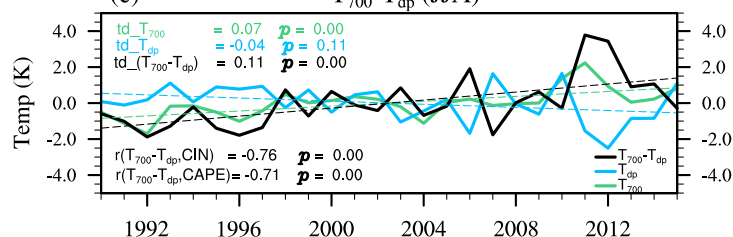
(a) Obs and Reg fine dust trend (1990-2015 JJA)



(b) CGP fine dust and influential factors (JJA)

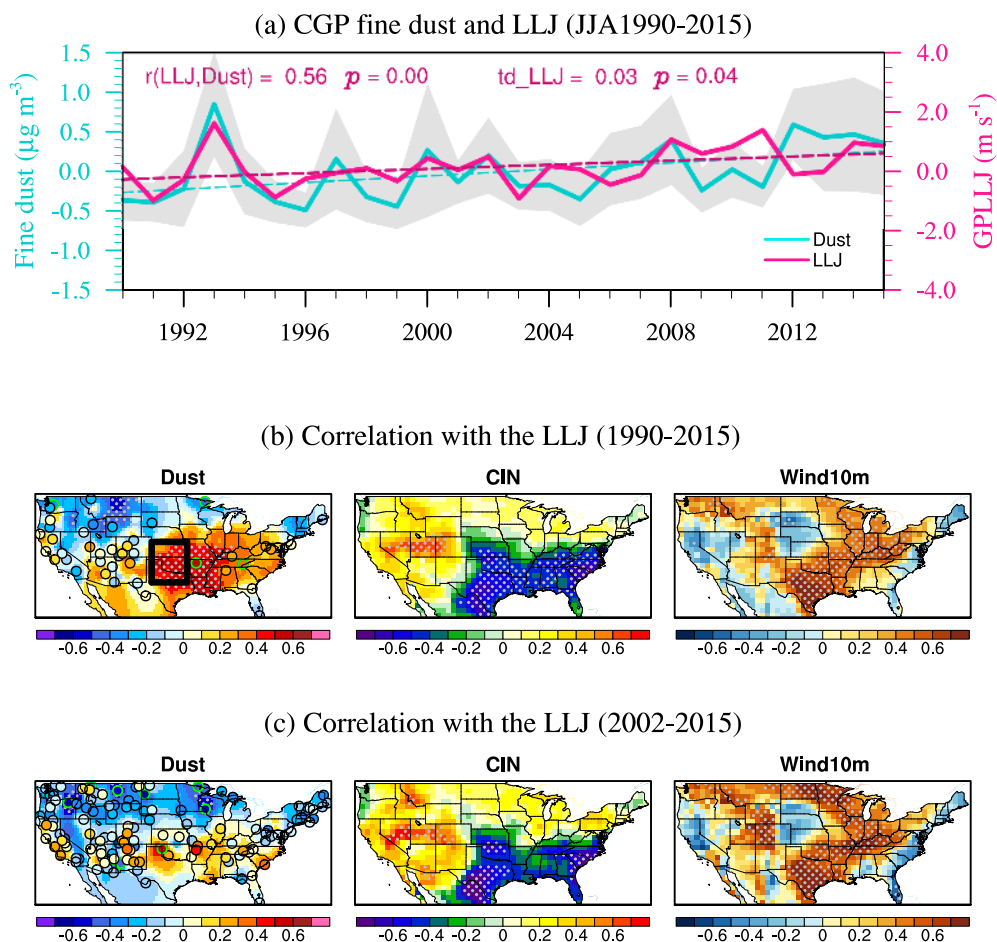


(c) $T_{700}-T_{dp}$ (JJA)



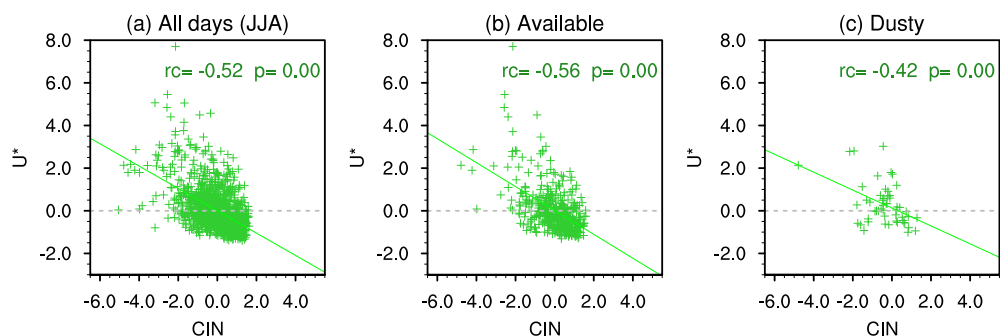
1018
 1019
 1020
 1021
 1022
 1023
 1024
 1025
 1026
 1027
 1028
 1029

Figure 4. (a) Observed (Obs) and reconstructed (Reg) trends of fine dust concentration ($\mu\text{g m}^{-3}$) using five factors in summer from 1990-2015. The contributions from each factor (precipitation, bareness, surface wind, CAPE, and CIN) are also shown (second and third rows). Dotted areas are significant at the 90% confidence level. Pattern correlation between reconstructed dust concentration trends and the observed trends are shown at the right corner of each plot. Black box denotes the central Great Plains (CGP). (b) Time series of fine dust concentration (cyan), CIN (orange), and CAPE (deep blue) averaged over the CGP and their linear trends (dashed lines). Gray shading denotes \pm one standard error of the observations. (c) Time series of $T_{700}-T_{dp}$ (black), T_{700} (green) and T_{dp} (light blue) and their linear trends (dashed lines) in summer from 1990 to 2015.



1030
 1031
 1032
 1033
 1034
 1035
 1036
 1037
 1038
 1039
 1040
 1041
 1042
 1043
 1044
 1045
 1046

Figure 5. (a) Time series of fine dust concentration ($\mu\text{g m}^{-3}$) averaged in the CGP (cyan) and the index of the Great Plains low-level jet (magenta) and their trends (dashed line) in JJA from 1990 to 2015. Gray shading denotes \pm one standard error of the observations. Correlations between the jet index and fine dust concentration, CIN, and near surface wind speed for (b) 1990-2015 and (c) 2002-2015. Colored circles denotes correlations at IMPROVE stations, with green outlines denotes the correlation is significant at the 90% confidence level. Areas significant at the 95% confidence level are dotted in (b) and significant at the 90% confidence level are dotted in (c).



1047

1048

1049 Figure 6. Scatter plot of standardized friction velocity (U^*) and CIN anomalies for (a) all
1050 days in JJA from 2002-2015, (b) days when fine dust data is available, and (c) dusty days
(when daily fine dust concentration anomaly is greater than one standard deviation).

1051

1052

1053

1054

1055

1056

1057

1058

1059

1060

1061

1062

1063

1064

1065

1066

1067

1068

1069

1070

1071

1072

1073

1074

1075

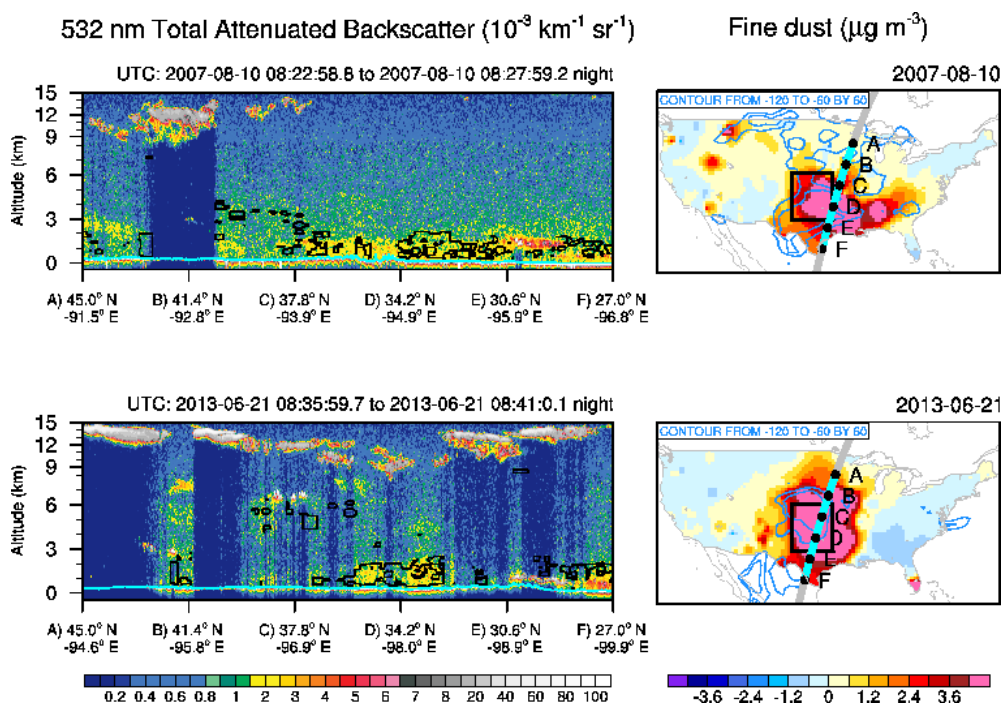
1076

1077

1078

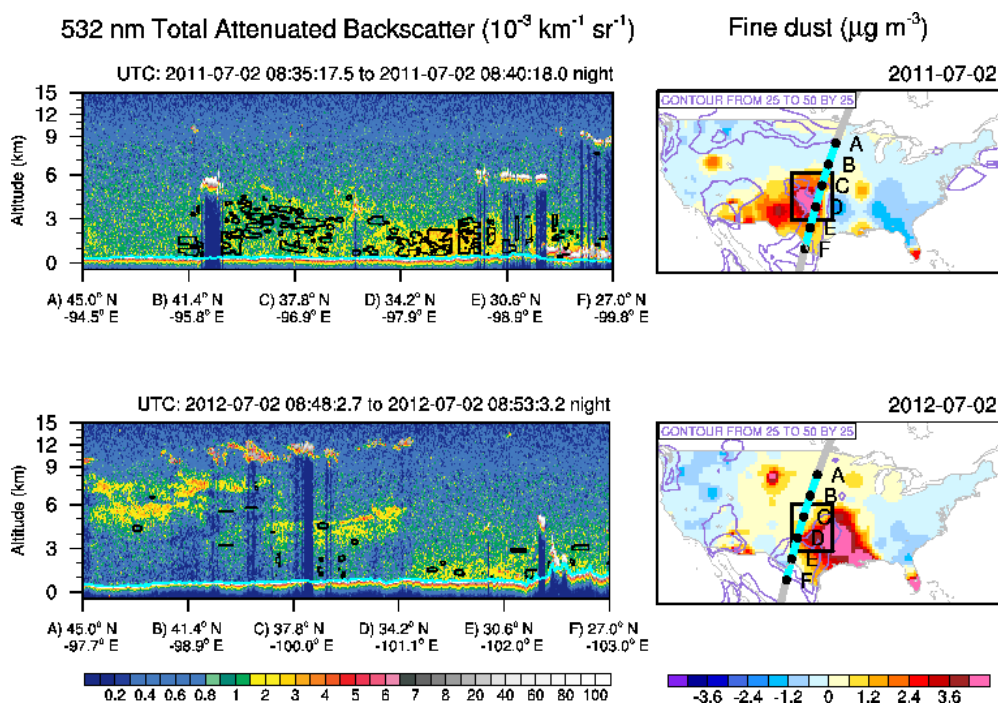
1079

1080



1081
 1082
 1083
 1084
 1085
 1086
 1087
 1088
 1089
 1090
 1091
 1092
 1093
 1094
 1095
 1096
 1097
 1098
 1099
 1100
 1101
 1102
 1103
 1104
 1105

Figure 7. Nighttime 532 nm total attenuated backscatter (shading) and depolarization ratio (black contours, values ≥ 0.2 are shown) from CALIOP on August 10th, 2007 (top left) and on June 21st, 2013 (bottom left), along with fine dust concentration anomaly ($\mu\text{g m}^{-3}$; shading, right column) and CIN anomaly (blue contour, only negative values from -60 to -120 J kg^{-1} are shown). CALIOP orbit tracks are shown in grey lines (right column) with cyan part and sampling points (A-F) denote the cross-section shown on the left column.

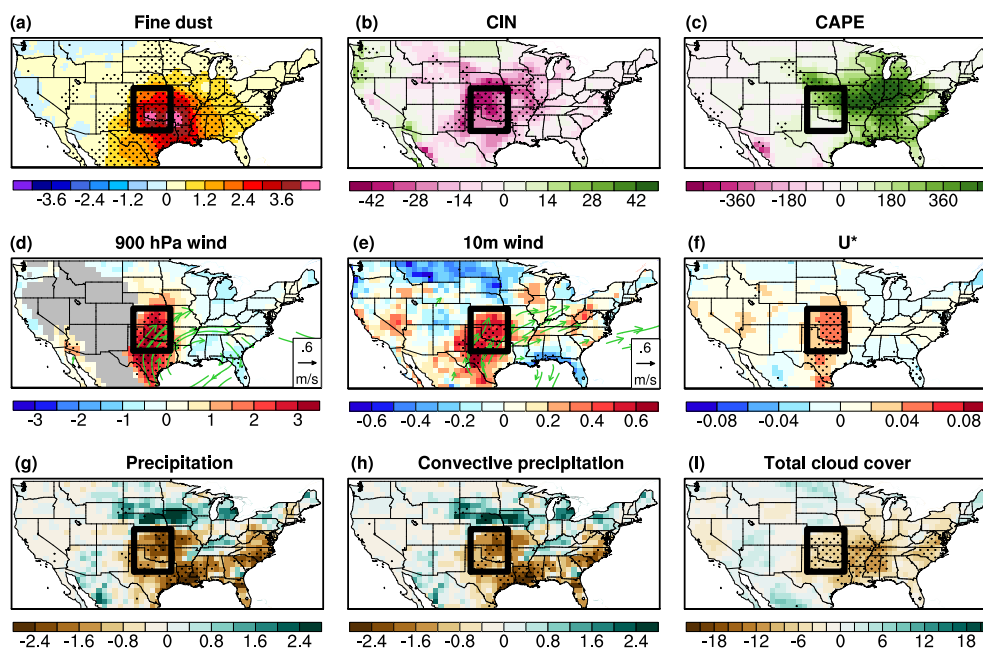


1106
 1107
 1108
 1109
 1110
 1111
 1112
 1113
 1114
 1115
 1116
 1117
 1118
 1119
 1120
 1121
 1122
 1123
 1124
 1125
 1126
 1127
 1128
 1129

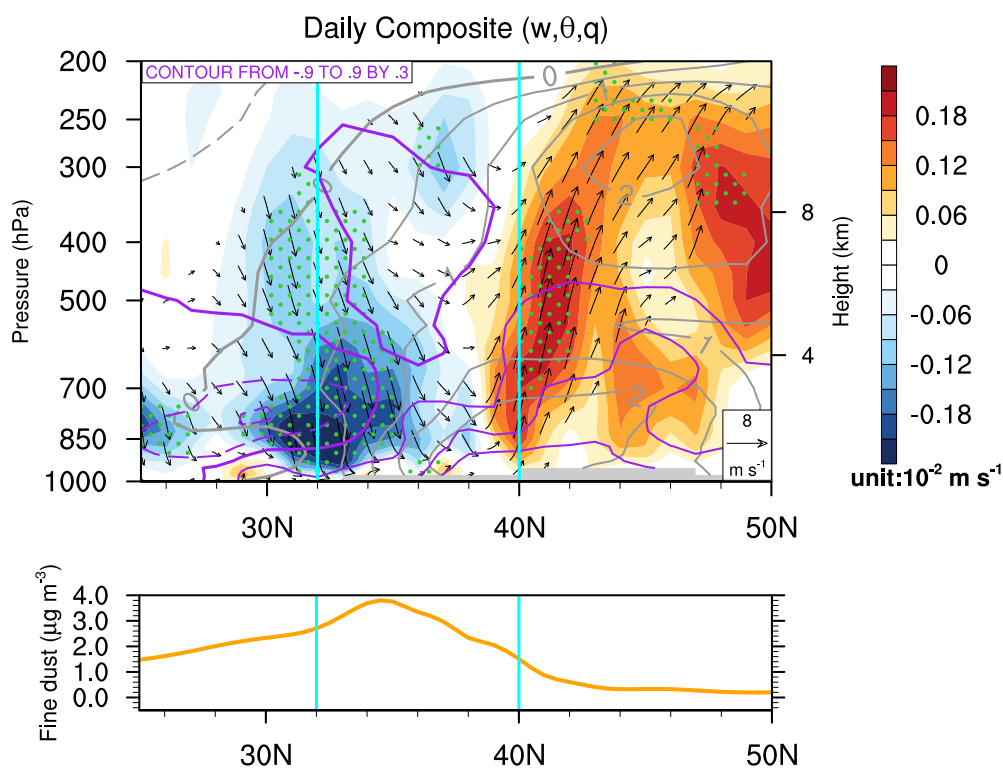
Figure 8. Same as Fig. 10 but for July 2nd, 2011 (top) and July 2nd, 2012 (bottom). Only positive CIN anomalies from 25 to 50 J kg⁻¹ are shown (light purple contour).



Daily composite (among JJA0215)

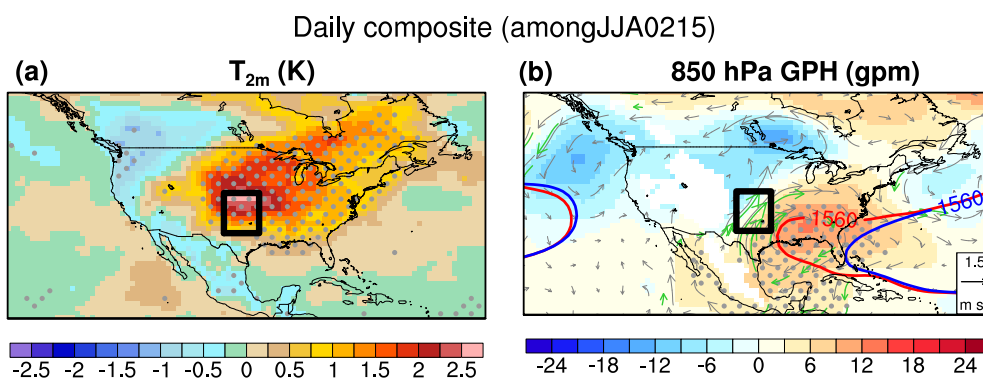


1130 Figure 9. Daily composites of the anomalies of (a) fine dust concentration ($\mu\text{g m}^{-3}$), (b)
1131 CIN (J kg^{-1}), (c) CAPE (J kg^{-1}), (d) 900 hPa wind speed (m s^{-1}), (e) 10 m wind speed (m
1132 s^{-1}), (f) U^* (m s^{-1}), (g) total precipitation (mm day^{-1}), (h) convective precipitation (mm
1133 day^{-1}), and (i) total cloud cover (%) during dusty days in JJA from 2002 to 2015. Dotted
1134 areas are significant at the 95% confidence level. 900 hPa and 10 m wind anomalies
1135 (green vectors) significant at the 95% confidence level are shown in (d) and (e).
1136
1137
1138
1139
1140
1141
1142
1143
1144
1145
1146
1147
1148
1149
1150
1151
1152



1153
1154 Figure 10. Daily composite of vertical velocity (shading; 10^{-2} m s^{-1}), potential
1155 temperature (grey contours; K), and specific humidity (purple contours; g kg^{-1}) from the
1156 ERA-Interim, and fine dust concentration anomalies (bottom; orange line) averaged
1157 between 95° and 102° W for dusty days in JJA from 2002 to 2015. Topography is
1158 masked out in grey. Cyan lines denote the domain of the CGP.
1159

1160
1161
1162
1163
1164
1165
1166
1167
1168
1169
1170
1171
1172
1173
1174
1175



1176
1177
1178
1179
1180
1181
1182
1183

Figure 11. Daily composites of (a) T_{2m} (K) and (b) 850 hPa geopotential height (gpm) and horizontal wind vectors (m s^{-1} ; grey) from the ERA-Interim averaged over dusty days in JJA from 2002-2015. Blue and red contours denote 1560 geopotential height in the climatology (2002-2015) and during dusty days, respectively. Areas significant at the 95% confidence level are dotted. Wind vectors significant at the 95% confidence level are plotted in green.